Volume 1 | Number 1 | Jan 2013 | Pages 1–100

Green Chemistry

Cutting-edge research for a greener sustainable future

www.rsc.org/greenchem

Stille couplings in water @RT

ROYAL SOCIETY OF CHEMISTRY

This is an *Accepted Manuscript*, which has been through the Royal Society of Chemistry peer review process and has been accepted for publication.

Accepted Manuscripts are published online shortly after acceptance, before technical editing, formatting and proof reading. Using this free service, authors can make their results available to the community, in citable form, before we publish the edited article. We will replace this *Accepted Manuscript* with the edited and formatted *Advance Article* as soon as it is available.

You can find more information about *Accepted Manuscripts* in the **Information for Authors**.

ROYAL SOCIETY OF CHEMISTRY

www.rsc.org/greenchem

1   **Microwave Promoted Continuous Flow Approach to Self-assembled**
2   **Hierarchical Hematite Superstructures**

3   M. K. Bayazit, E. Cao, A. Gavriilidis and J. Tang*

5   Department of Chemical Engineering, University College London, Torrington Place, London,
6   WC1E 7JE, UK

8   **Abstract**

9   In this work a microwave promoted flow (MWPF) system to reproducibly synthesize self-

10   assembled hierarchical hematite superstructures (Hem-SSs) using sole precursor

11    $(Fe(NO_3)_3 \cdot 9H_2O)$ and single mode microwave in aqueous conditions has been developed. The

12   functional characterisation by XRD, (HR)TEM, XPS, UV-vis and Raman spectroscopies

13   proved that highly crystalline ellipsoid Hem-SSs (~180 nm × 140 nm) were produced, built

14   from primary hematite nanoparticles, 5–10 nm in size using 0.05 mol L^{-1} precursor

15   concentration, 1 mL min^{-1} flow rate and short reaction time (about 6 min). Particles produced

16   via conventional heating (CH) at 120 and 140 °C in the same flow reactor under similar

17   experimental conditions were found to consist of mixtures of goethite and hematite. The

18   effects of precursor concentration (0.1 and 0.2 mol L^{-1}) and flow rate (2 and 5 mL min^{-1}) on

19   Hem-SSs were further investigated and the synthesis mechanism was also discussed. This

20   novel method opens a window for continuous fabrication of metal or metal oxide

21   nanoparticles/superstructures by a green approach to meet industrial requirement.

22

23

24

25

1   **Introduction**

2   Highly-ordered superstructures, so-called mesocrystals, formed via hierarchical self-assembly

3   of primary nanoparticles (NPs) following a non-classical crystallization route are interesting

4   materials due to their distinctive properties including enhanced surface area, accessible pores

5   and tunable electronic, optical and magnetic properties that make them potentially applicable

6   in catalysis, paints, sensors and electronics.[1-4] Metal oxide superstructures have recently been

7   reviewed, with particular attention on their use for energy conversion and storage

8   applications.[5] Among them, highly oriented hematite superstructures (Hem-SSs) have

9   attracted specific attention due to their excellent lithium insertion,[6, 7] photocatalytic

10   performance[8] and improved sensing properties[9] compared to hematite single crystals.

11   Platelike α-Fe$_2$O$_3$ mesocrystals were used as a support to prepare gold loaded platelike α-

12   Fe$_2$O$_3$ mesocrystals that were shown to be highly efficient and stable catalyst for CO

13   conversion compared to commercially available α-Fe$_2$O$_3$ sample (Fluka).[9] Higher activity

14   was attributed to the significant increase in the (110) diffraction intensity for the platelike α-

15   Fe$_2$O$_3$ mesocrystal support.[9] Furthermore, high temperature (400 °C) annealed platelike α-

16   Fe$_2$O$_3$ mesocrystals showed enhanced gas-sensing sensitivity compared to commercial α-

17   Fe$_2$O$_3$, probably due to highly-oriented and crystalline α-Fe$_2$O$_3$ superstructures.[9] Similarly,

18   as-prepared rhombic α-Fe$_2$O$_3$ mesocrystals were tested for lithium storage capacity that

19   demonstrated improved cycling stability for 5-50 cycles with storage capacity of 756 mA h g$^-$

20   ^{1} after 50 cycles, probably due to the closed and intracrystalline porosity, compared to single-

21   crystal α-Fe$_2$O$_3$ that showed gradual loss of capacity after ~20 cycles.[6]

22   Hematite is an n-type semiconductor (E$_g$=2.1 eV) with rhombohedral crystal structure and is

23   weakly ferromagnetic at room temperature.[10] Hematite (α-Fe$_2$O$_3$) as a precursor can also be

24   converted into other useful forms of iron oxide such as maghemite (γ-Fe$_2$O$_3$) and magnetite

25   (Fe$_3$O$_4$).[11] Hematite nanoparticles (Hem-NPs) can be synthesized conventionally by several

1 techniques including hydrothermal/solvothermal,[12, 13] sol-gel processing[14] and chemical vapor

2 deposition methods,[15] using predominately a batch reactor or a large tubular reactor.

3 Alternatively, a microwave-assisted hydrothermal batch reactor can be employed to prepare

4 nanosized hematite particles as catalysts and adsorbents using both $Fe(NO_3)_3$ (0.1 mol L^{-1})

5 and urea (0.5 mol L^{-1}) as precursors.[16]

6 Mesocrystals or superstructures of hematite can be prepared by a complicated self-assembly

7 of primary hematite nanoparticles. In these processes, organic surfactants or templates are

8 crucial to form surface stabilized primary Hem-NPs that prevent particle-particle fusion

9 during mesocrystal formation. However, these additives are likely to decompose into

10 hazardous materials at high reaction temperatures and long reaction times.

11 For example, porous plate-like hematite mesocrystals with a dimension of 100-400 nm were

12 synthesized by self-assembly of *in-situ* prepared Hem-NPs (5-15 nm) in an ionic liquid

13 [Bmim]Cl, acting as both solvent and templating agent, via a controlled solvent evaporation

14 process reacting $FeCl_3.6H_2O$, water and *n*-butylamine in air at 120 °C for 20 h.[9]   Similarly,

15 olive-like photocatalytically active Hem-SSs with size 620 nm × 940 nm have recently been

16 prepared via self-assembly of primary hematite nanoparticles (5-10 nm) using $FeCl_3$ and silk

17 fibroin as a biotemplate in water by heating at 160 °C for 10 h.[8] A solvothermal approach

18 was used to prepare high-stability hematite mesocrystals from $Fe(NO_3)_3.6H_2O$ in *N,N*-

19 dimethylformamide (DMF) and methanol (MeOH) mixture with varying amounts at 180 °C

20 for 24 h.[6] It was proposed that the intermediate $NH_2(CH_3)_2^+$ acted as stabilizer for primary

21 hematite particles and higher amount of methanol conditions produced rhombic

22 (DMF:MeOH; 20:5, v/v) or ellipsoidal (DMF:MeOH; 17:8, v/v) mesocrystals. A

23 hydrothermal method at 200 °C for 12 h in ethanol/water mixture (9:1, v/v) to synthesize

24 elliptic single-crystalline hematite superstructures was also reported.[7]

1   Although the abovementioned methods had their own advantages (*e.g.* controlling shape and

2   growth direction of superstructures *etc.*) they obviously required additional chemicals (*e.g.*

3   reducing agents, surfactants, templates or stabilizers). Furthermore, it is challenging to scale

4   those processes up while retaining the same structure/properties due to long reaction times,

5   limited reactor capacity, high-energy consumption and low product yields. To meet the

6   increasing demand in highly stable, self-assembled, hierarchical superstructures with defined

7   shapes for diverse applications, a green, reproducible and energy/cost efficient technique is

8   desirable, which is also scalable. For this purpose, microwave heating (MH) coupled with

9   continuous flow synthesis may offer an attractive route for the rapid, continuous and

10   controlled growth of self-assembled stable metal oxide superstructures. The use of continuous

11   micro/milliflow technology has gained significant attention in recent years owing to large

12   surface-to-volume ratio that depresses the diffusion times of chemical species.[17-21]

13   Microfluidic systems have been successfully utilized with CH to carry out chemical reactions

14   and nanocrystal preparation due to their versatility to perform rapid mixing, controllable mass

15   and heat transfer under continuous flow conditions.[17] Local variations in reaction conditions

16   such as concentration, temperature and reaction time are likely to have significant effect on

17   both nucleation and particle growth, and a better control over these variables may improve

18   the monodispersity, particle size and its distribution, shape and morphology, crystallinity and

19   purity of nano-particles manufactured, which MH could provide due to its fast and selective

20   heating.

21   Herein, continuous manufacturing of self-assembled hierarchical ellipsoid hematite

22   superstructures (Hem-SSs) with an average dimension of ~100-200 nm using a microwave

23   promoted continuous flow approach in an aqueous solution using $Fe(NO_3)_3.9H_2O$ as the only

24   precursor is presented for the first time. The effect of precursor concentration and flow rate

25   on the geometry and morphology of the formed particles were investigated. The results

1 obtained by MH were also compared with the results of particles produced by CH under

2 similar reaction conditions. Furthermore, the reproducibility of the process was examined.

3 **Experimental**

4 **Synthesis of Hematite Nanoparticles.** All chemicals were purchased from Sigma-Aldrich

5 and used as received. The microwave promoted continuous flow method consisted of a flow

6 reactor (6 mL) made of 1/8" PTFE tubing, a CEM single-mode microwave system, a syringe

7 pump, a temperature probe positioned at the exit of reactor, a sample/waste collection unit

8 with backpressure regulator and an ice-bath. For the synthesis of particles using CH, the

9 microwave instrument was replaced by a thermal bath using glycerol as a heating medium. In

10 a typical procedure, a 50 mL syringe filled with 0.1 mol L^{-1} of iron (III) nitrate nonahydrate

11 $(Fe(NO_3)_3.9H_2O, 99.9\%)$ solution (pale yellow in color) dissolved in deionized water at

12 room temperature was connected to the flow reactor and the reactor was filled with the

13 precursor solution. The pressure of the flow reactor was adjusted at 20 psi using a pressurized

14 air cylinder. Pressure adjustment was provided via air controlled by a pressure regulator (20

15 psi) with a gas escape route immersed in a water bath. The precursor was pumped into the

16 flow reactor at a flow rate of 1 mL min^{-1} and pre-adjusted microwave irradiation (40 W) was

17 applied simultaneously. After 8 min, the temperature probe displayed a constant temperature

18 value (~119-120 °C) and 8 mL of the pumped solution was collected in waste collection unit.

19 Thereafter, the main product mixture passed through an ice-bath to cool down below room

20 temperature and was collected in a sample collection unit. The mixture was centrifuged at

21 2500 rpm for 90 min to recover the particles formed. Recovered particles were washed by

22 deionized water and re-centrifuged, isolated and dried at room temperature for

23 characterization.

24 **Materials Characterization.**The X-ray diffraction (XRD) patterns of samples were obtained

25 with a Bruker D8 Advance Powder X-ray diffractometer with a Mo-K_α (λ=0.71 Å) radiation

1　source. Diffraction patterns were collected from 10° to 70° and a step size of 0.002 °/s was

2　used. Field emission scanning electron microscopy (FESEM) was employed to observe the

3　size and shape of the nanomaterials, using a JEOL JSM-7401F operating at 3-5kV. Materials

4　were tested in powder form prepared from ethanol dispersions. UV/Vis spectra were obtained

5　from stable dispersions of produced particles in ethanol using a Shimadzu UV-2550 UV/Vis

6　spectrophotometer. High-resolution XPS was performed by a Thermo Scientific K-alpha

7　photoelectron spectrometer with monochromatic Al-K_α radiation; peak positions were

8　referenced to C 1s line at 284.5 eV and the CasaXPS software was used for data processing.

9　Transmission electron microscopy (TEM) and high resolution transmission electron

10　microscopy (HRTEM) were performed using Jeol JEM-1010 and JEOL-2010F coupled with

11　an EDS detector (Oxford Instruments) instruments, respectively. TEM samples were prepared

12　from stable dispersions of particles prepared in ethanol by dropping on carbon coated copper

13　grids. Particle size distribution was estimated from TEM data measuring particle size using

14　ImageJ. All graphs and statistical analysis were obtained by OriginLab software (Origin9.1).

15　**Results and discussion**

16　**Preparation of HEM-SSs.** Highly pure and crystalline Hem-SSs, reddish-brown in color,

17　were successfully fabricated via a cheap and readily available precursor, $Fe(NO_3)_3.9H_2O$,

18　under flow conditions. Unlike previously reported conventional and microwave-assisted

19　hydrothermal batch processes,[6, 8, 9, 16] MWPF synthesis of Hem-SSs does not require any

20　reducing agent (*e.g.* urea), surfactant or template. The potential by-products have a high

21　solubility in water (e.g. HNO_3), facilitating the isolation/purification of synthesized ellipsoid

22　Hem-SSs, thus low speed centrifugation was applied. Hem-SSs were produced at 120 °C

23　under 40 W fixed MW power, 1 mL min^{-1} flow rate and 20 psi applied back pressure. It is

24　also worth noting that the temperature value (120 °C) was recorded outside the MH zone

25　using a temperature probe positioned *ca.* 5 cm away from the reactor exit from the

1   microwave irradiated zone. Thus, the inside temperature of the flow reactor is likely to be

2   somewhat higher than that of the recorded temperature outside the microwave cavity. The

3   current configuration of the reactor and small microwave cavity make the measurement of the

4   temperature of hot fluid inside the reactor very difficult. In order to make our comparison

5   more accurate, we estimated the temperature at the exit of the microwave irradiated zone,

6   taking into account the heat transfer between the fluid inside the PTFE tubing and the outside

7   surrounding air (**See ESI for calculations**). The estimated fluid temperatures at the exit of

8   the microwave irradiated zone for different fluid flow rates are listed in Table 1. It can be

9   seen that the temperature difference between the inside temperature near the exit and the

10   measured is quite small, less than 7 $^{\circ}$C at the current conditions.

11   Table 1 Estimated fluid temperature at the exit of the microwave irradiated zone

Fluid volume flow rate (F), mL min^{-1}	Fluid mass flow rate (m), g s^{-1}	Temperature at the exit of the microwave irradiated zone ($t_{i,MW}$), $^{\circ}$C
1	0.01663	126.7
2	0.03327	123.3
5	0.08317	121.3

12

13   The X-ray diffraction (XRD) patterns of iron oxide particles prepared by the MWPF system

14   using different concentrations (0.05, 0.1 and 0.2 mol L^{-1} precursor) show the presence of

15   characteristic hematite (α-Fe$_2$O$_3$) peaks (**Figure 1a**). In contrast, an inseparable mixture with

16   poor crystallinity, attributed to the mixture of hematite and goethite particles indicated by

17   XRD, was obtained when the reaction was conducted by CH using 0.1 and 0.2 mol L^{-1}

18   Fe(NO$_3$)$_3$.9H$_2$O precursor concentrations at 120 $^{\circ}$C and even 140 $^{\circ}$C (not shown) (**Figure**

19   **1a**). When the precursor concentration was decreased to 0.05 mol L^{-1} Fe(NO$_3$)$_3$.9H$_2$O, no

20   particles were isolated when reaction was performed by CH at 120 $^{\circ}$C. On the other hand,

21   highly pure and crystalline hematite particles were obtained (confirmed by sharp and narrow

22   XRD peaks) when 0.05 M Fe(NO$_3$)$_3$.9H$_2$O precursor was used (**Figure 1a**). The observed

23   XRD peaks for Hem-SSs (ICSD—96075) were assigned to Miller's indices of [012], [104],

1 [110], [113], [202], [024], [116], [018], [214], [300], [208], [1010], [220], [306], [223], [312],

2 [0210], [134], [315] and [2110]. When high concentration of precursor (0.1 and 0.2 mol L^{-1}

3 Fe(NO$_3$)$_3$.9H$_2$O) was used, Hem-SSs were again produced successfully. However, slightly

4 broadened XRD peaks were observed, suggestive of less crystalline hematite particle

5 formation possibly due to insufficient microwave energy provided. XRD results reveal that

6 the degree of crystallinity of the MWPF system synthesized Hem-SSs was related to the

7 precursor concentration. Low precursor concentrations yielded highly crystalline hematite

8 preparation.

9 The oxidation state of Fe in Hem-SSs prepared by MWPF using 0.05 mol L^{-1} Fe(NO$_3$)$_3$.9H$_2$O

10 precursor was further analyzed by XPS. Previous studies for α-Fe$_2$O$_3$ reported two main

11 peaks positioned at *ca.* 724 and 711 eV, attributed to Fe 2p$_{1/2}$ and Fe 2p$_{3/2}$, respectively.[22] It

12 was also shown that the latter one was narrower and stronger[23] and these peaks were clearly

13 accompanied by satellite structures on their high binding-energy side, at about 8 eV.[22]

14 Consistent with previous literature, XPS analysis of Hem-SSs displayed four peaks at *ca.*

15 733, 724, 719 and 711 eV, confirming the synthesis of pure hematite structures (**Figure 1b**).

16
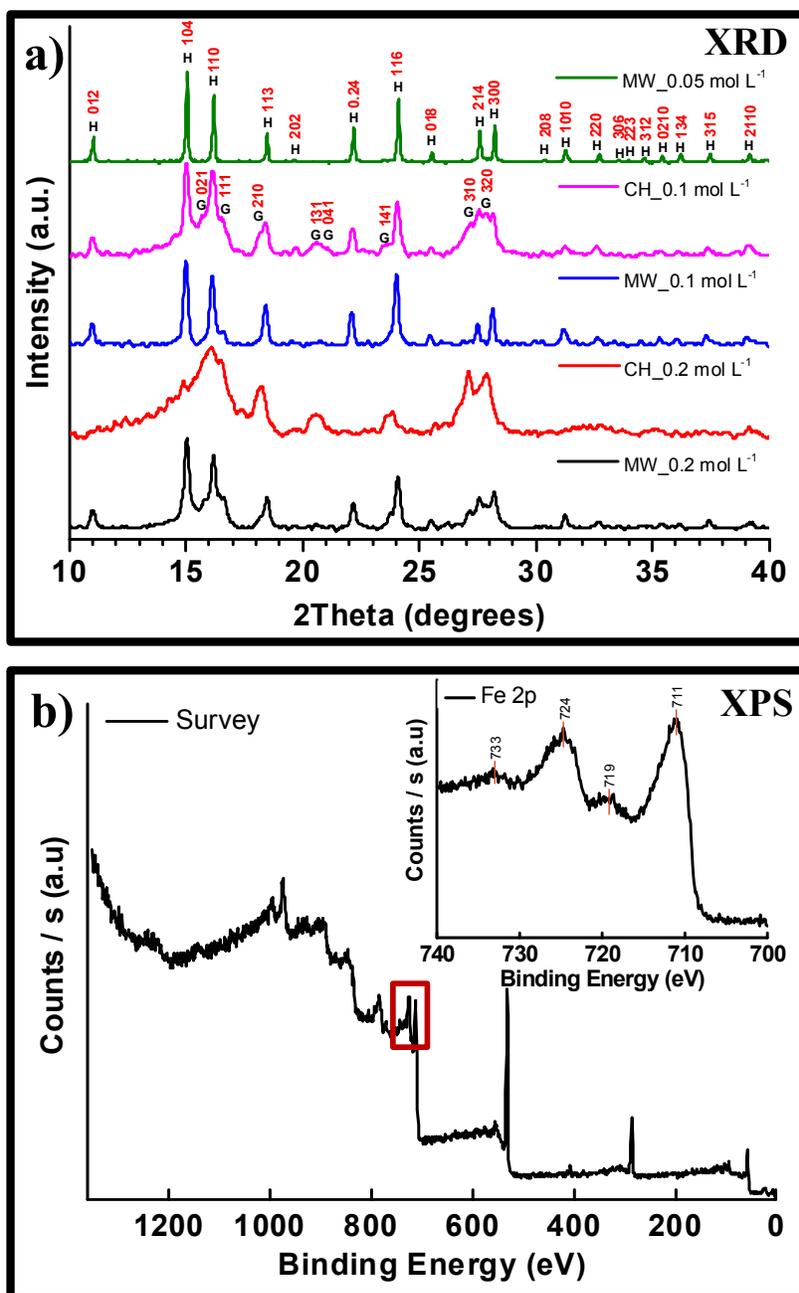
Figure 1 (a) XRD patterns of MH and CH assisted flow system synthesized particles at 120 °C using 0.05, 0.1 and 0.2 mol L^{-1} $Fe(NO_3)_3.9H_2O$ precursor. Molybdenum K-alpha (λ=0.71 Å) was used as a source. 'G' corresponds to goethite. **(b)** XPS spectrum of MWPF synthesized Hem-SSs at 1 mL min^{-1} flow rate (Reactor volume: 6 mL) using 0.05 mol L^{-1} $Fe(NO_3)_3.9H_2O$ precursor. Inset: Expanded Fe 2p XPS spectrum of Hem-SSs.

1   Absorption spectroscopy has been widely used to characterize hematite particles in solution

2   and solid state.[23, 24] As expected, UV-vis spectra of isolated Hem-SSs show an absorption

3   band at *ca.* 390 nm and a weak shoulder at *ca.* 530 nm, characteristic of pure hematite,

4   compared to $Fe(NO_3)_3.9H_2O$ precursor (**Figure 2**).
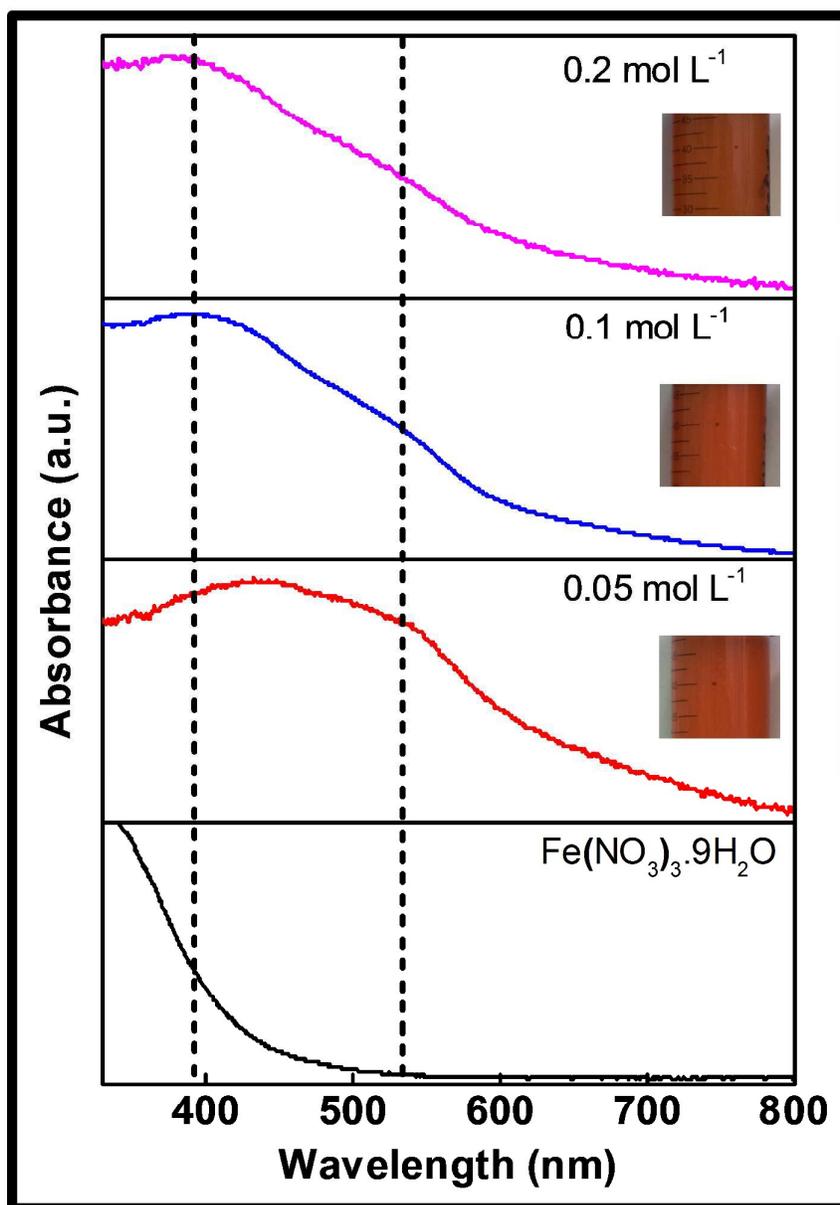
5

6   **Figure 2** Photos and absorption spectra of MWPF system synthesized Hem-SSs using 0.05,

7   0.1 and 0.2 mol L^{-1} $Fe(NO_3)_3.9H_2O$ precursor, and pure $Fe(NO_3)_3.9H_2O$ precursor.

1   Furthermore, it was noticed that the characteristic absorption bands of Hem-SSs prepared by

2   0.05 mol L^{-1} Fe(NO$_3$)$_3$.9H$_2$O precursor were red-shifted by ~20 nm compared to 0.1 and 0.2

3   mol L^{-1} precursor concentration. Although this type of shift is generally attributed to larger

4   particle size, it may also be due to high crystallinity of the produced particles using 0.05 mol

5   L^{-1} precursor, coinciding with XRD patterns of these samples.[25]   Conversely, no clear

6   hematite related absorption band was observed for the isolated particles produced by CH at

7   120 ^{o}C using 0.1 mol L^{-1} Fe(NO$_3$)$_3$.9H$_2$O precursor in a flow reactor although XRD pattern

8   (please see Figure 1a) of isolated particles revealed a mixture of goethite and hematite

9   particles (**ESI Figure S1**). On the other hand, consistent with observed XRD peaks, the

10   isolated particles produced by CH at 120 ^{o}C using 0.2 mol L^{-1} Fe(NO$_3$)$_3$.9H$_2$O precursor

11   showed an absorption band at *ca.* 400 nm, probably due to the presence of relatively high

12   concentration of hematite particles in isolated mixture, compared to 0.1 mol L^{-1}

13   Fe(NO$_3$)$_3$.9H$_2$O precursor. Assuming that the temperature of the reactor in the microwave

14   cavity was somewhat higher than 120 ^{o}C as predicted by our calculations, the reaction was

15   further performed by CH at 140 ^{o}C using 0.1 mol L^{-1} Fe(NO$_3$)$_3$.9H$_2$O precursor. However, no

16   characteristic hematite related UV-vis absorption bands at *ca.* 390 and 530 nm were obtained,

17   suggesting that pure hematite particles could not be prepared by CH at 120 and 140 ^{o}C under

18   similar experimental conditions (**ESI Figure S1**). All these are consistent with results

19   obtained by XRD measurements.

20   Transmission electron microscopy (TEM) provided insight into the morphology, particle size

21   distribution and sub-units of Hem-SSs. TEM images of hematite particles prepared using

22   0.05, 0.1 and 0.2 mol L^{-1} Fe(NO$_3$)$_3$.9H$_2$O show ellipsoid hematite structures with particle size

23   (length/width) distribution of 180±92 nm/140±67 nm, 124±62 nm/75±33 nm and 112±69

24   nm/73±34 nm, respectively (**Figure 3a-f**). Close inspection of TEM image of ellipsoid

25   hematite particles reveals that each particle has relatively rough surfaces and is composed of

1   highly oriented or self-assembled primary hematite particles, with boundaries between them

2   (**Figure 3g**). The presence of clear particle-particle boundaries suggest that subunits of Hem-

3   SSs are not fused and they might be dispersed by applying external forces (*e.g.* sonication,

4   mechanical stirring *etc.*).

5
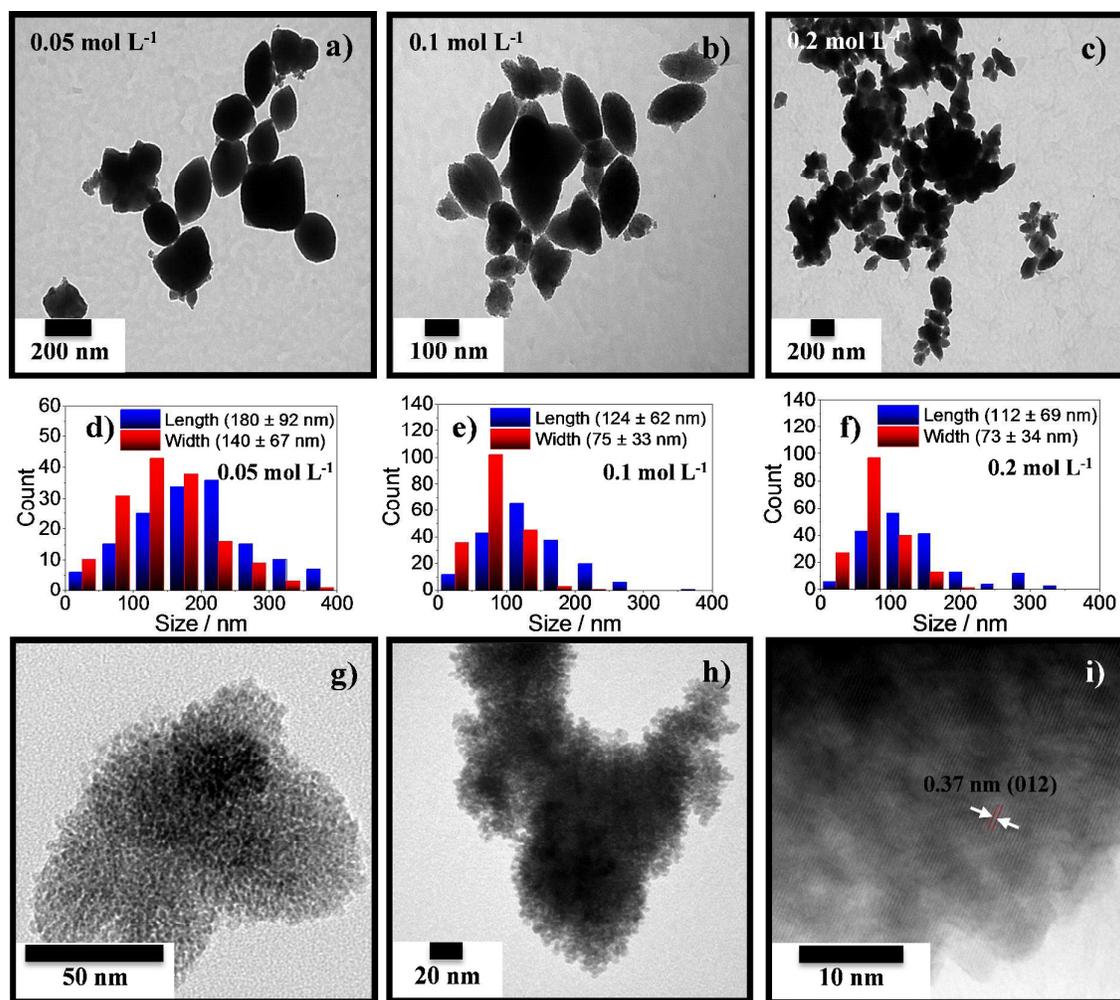
6

7   **Figure 3** TEM images of MWPF system synthesized ellipsoid Hem-SSs using 0.05, 0.1 and

8   0.2 mol L^{-1} Fe(NO$_3$)$_3$.9H$_2$O precursor and (**a-c**) particle size distribution (length/width) of

9   ellipsoid Hem-SSs (**d-f**). TEM images of MWPF synthesized ellipsoid Hem-SSs before (**g**)

10   and after (**h**) mild sonication using 0.05 mol L^{-1} Fe(NO$_3$)$_3$.9H$_2$O precursor. HRTEM image of

11   ellipsoid Hem-SSs using 0.05 mol L^{-1} Fe(NO$_3$)$_3$.9H$_2$O precursor (**i**).

1   Thus, mild sonication (750 W sonic probe, 40% amplitude) was applied to ellipsoid Hem-SSs

2   in ice cooled ethanol for 5 min. High-resolution TEM (HR-TEM) images of mildly sonicated

3   Hem-SSs show partial exfoliation of uniform granular primary hematite nanocrystals

4   approximately 5-10 nm in size (**Figure 3h**), suggesting that interaction between the subunits

5   is relatively strong. Furthermore, it is worth noting that the ellipsoid morphologies of Hem-

6   SSs are preserved, suggestive of highly-ordered stable superstructure. The lattice fringes in a

7   typical HRTEM image (**Figure 3i**) are separated by ~3.7 Å, which agrees well with the [012]

8   lattice spacing of hematite and further confirm that α-Fe_2O_3 NPs (*e.g.* crystallinity) are not

9   altered via mild sonication. It is also worth noting that HRTEM analysis of α-Fe_2O_3

10   mesocrystals prepared by conventional heating in previous literature using both

11   $Fe(NO_3)_3.9H_2O$[6] and $FeCl_3.6H_2O$[9] exhibited lattice fringes separated by ~2.5 Å, attributed to

12   [110] facet as compared to Hem-SSs with [012] facet prepared by MWPF system. This

13   probably suggests that microwave heating induces crystal growth along the [012] direction. It

14   is therefore believed that mesocrystals prepared by MWPF system may show unusual

15   activities due to their different crystal facet and lattice spacing that may provide more

16   accessible surface compared to conventionally prepared mesocrystals.[6, 9] On the other hand,

17   no ellipsoid pure hematite was observed by TEM analysis of particles prepared by CH (**ESI**

18   **Figure S2**). HRTEM image of samples showed ~10 nm particles with irregular shapes and

19   lattice spacing of ~2.0, 2.4 and 2.7 Å, corresponding to [131] lattice spacing of goethite, and

20   [104] and [110] lattice spacing of hematite, respectively, further confirming that CH mainly

21   produced a mixture of hematite and goethite nanoparticles. Overall (HR)TEM analysis of

22   Hem-SSs suggests that MWPF system is able to produce highly stable and ordered Hem-SSs.

23   **Effect of Reactant Flow Rate on Synthesis of Hem-SSs.** The effect of reactant flow rate on

24   the physical properties of the particles was studied by TEM, UV-vis and Raman

25   spectroscopy. Typical reaction conditions (120 °C, 0.1 mol L^{-1}, 6 mL reactor) and applied

1   back pressure (20 psi) were kept constant and the reaction was carried out at flow rates of 1, 2

2   and 5 mL min^{-1}, where 1 mL min^{-1} was the minimum reliable flow rate in the current

3   configuration. No visible particle formation was observed at 2 and 5 mL min^{-1} flow rates.

4   Thus, the isolated hematite particles for 1 mL min^{-1} flow rate and soluble crude mixtures for 2

5   and 5 mL min^{-1} flow rates were used for bulk UV-vis and Raman analysis. UV-vis spectrum

6   of the isolated particles synthesized at 1 mL min-1 flow rate showed the characteristic

7   hematite absorption bands while

8
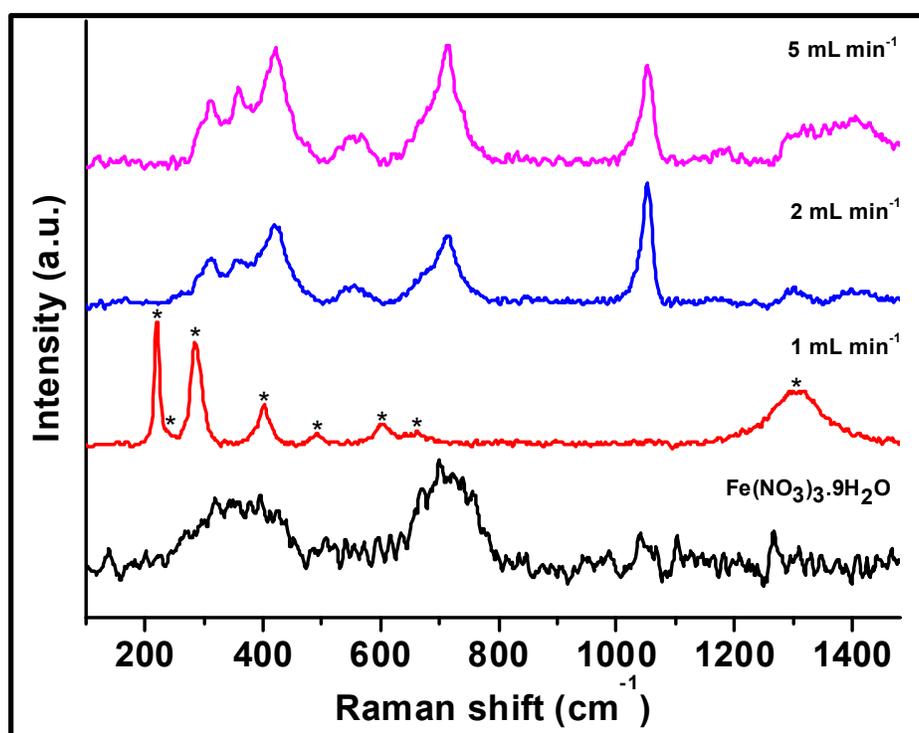
9   **Figure 4** Raman spectra of MWPF system synthesized ellipsoid Hem-SSs using 0.05 mol L^{-1}

10   Fe(NO$_3$)$_3$.9H$_2$O precursor at 1, 2 and 5 mL min^{-1} flow rate, and pure Fe(NO$_3$)$_3$.9H$_2$O

11   precursor for comparison. * corresponds to the characteristic hematite related Raman shifts.

12   the crude mixtures prepared at higher flow rates showed no clear bands (**ESI Figure S3**). In

13   agreement with previous literature,[26, 27] Raman spectra of Hem-SSs prepared via 1 mL min^{-1}

14   flow rate displayed characteristic hematite (α-Fe$_2$O$_3$) Raman shifts at *ca.* 201, 240, 285, 401,

1   492, 601, 665 and 1300 cm^{-1}, compared to precursor signals positioned at 356 and 712 cm^{-1}

2   (**Figure 4**). In contrast, reaction mixtures obtained at 2 and 5 mL min^{-1} flow rates showed no

3   hematite related Raman shifts, suggesting that low residence times (3 min for 2 mL min^{-1} and

4   1.2 min for 5 mL min^{-1}) were not enough to produce hematite particles (**Figure 4**). Further

5   TEM analysis of crude reaction product (2 mL min^{-1} flow rate) showed a mixture of small

6   particles 1-2 nm in size, some ellipsoid (~200 nm in length) and spherical (~100 nm or less)

7   particles, suggesting that the minimum residence time required to prepare pure ellipsoid

8   Hem-SSs should probably be at *ca.* 6 min (1 mL min^{-1}) under the experimental conditions

9   utilized (**ESI Figure S4**). Furthermore, no ellipsoid particle formation was observed at 5 mL

10   min^{-1} flow rate although some non-hematite spherical particles, confirmed by Raman

11   analysis, (~20-30 nm and ~1-2 nm in size) were observed.

12   **Reproducibility of Synthesis.** Reproducibility of the MWPF process was tested by repeating

13   the fabrication of Hem-SSs two more times under the same experimental conditions using 0.1

14   mol L^{-1} Fe(NO$_3$)$_3$.9H$_2$O precursor at 1 mL min^{-1} flow rate. Isolated Hem-SSs were

15   characterized by TEM. In all cases TEM analyses showed ellipsoid Hem-SSs with particle

16   size distribution of ~130 nm (length) and 80 nm (width), confirming that the developed

17   synthesis method is reproducible and capable of producing Hem-SSs with similar size

18   distributions (**Figure 5**).
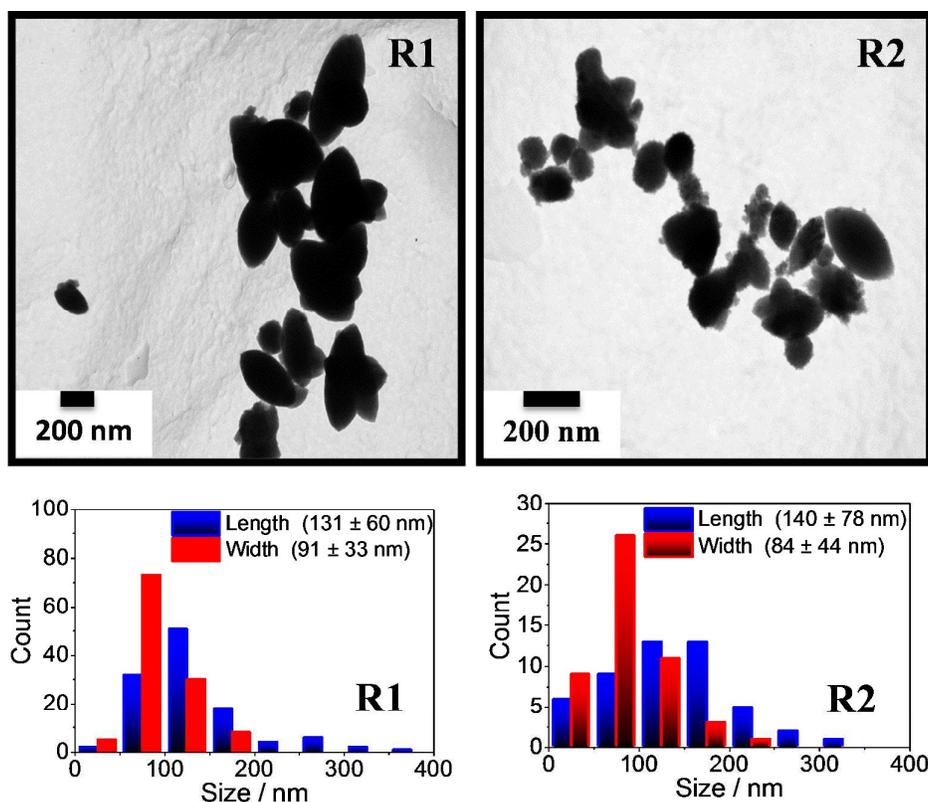
1

2 **Figure 5** TEM images of ellipsoid Hem-SSs produced by two different repeat experiments

3 (R1 and R2) under the same experimental conditions and the particle size distribution of the

4 produced Hem-SSs.

5 **Mechanism of Hem-SSs Formation.** In agreement with previous literature,[8] the morphology

6 of hematite particles is thought to be an oriented growth with primary nanoparticles. In

7 general, mesocrystal formation mechanisms are described by the hierarchical self-assembly

8 of primary nanoparticles following a non-classical crystallization route that is based on either

9 self-assembly or ligand-directed assembly of well-aligned small nanoparticles.[1-4] During the

10 formation of well-oriented superstructures, an equilibrium state is however essential between

11 the interparticle interactions including the dipole-dipole attraction, van der Waals interaction

12 and the double layer repulsion for directed self-assembly of colloidal particles.[28, 29] This type

13 of balance can be facilitated by an external electric or magnetic field if sufficient dipole–

14 dipole interactions are induced.[28, 29] In addition, self-assembly of nanostructures was also

1   shown in fluidic reactors that provide small reaction volumes and laminar flow,

2   facilitating the fine-adjustment of mixing rates, shear forces and reagent

3   concentrations.[30, 31]

4   Regarding the formation of ellipsoid Hem-SSs, the multiple effects induced by shear force

5   due to fluid flow and continuously exerted microwave irradiation might have played the key

6   roles, since no other templates/surfactants/organic solvents are present in our reaction system.

7   The shear induced aggregation of nanoparticles can be described by the dimensionless

8   Péclet number; shear forces have a stronger influence on aggregation for high flow Péclet

9   numbers ($P_e \geq 1$).[30] The flow Péclet number for the dilute solutions of α-Fe$_2$O$_3$ NPs using

10   particle size of ~10 nm (estimated by TEM) is 2.74×10^{-6}, suggesting that self-assembly of

11   hematite primary particles was not probably due to shear induced aggregation.[30, 32] (*see ESI*

12   *for calculations*)

13   Considering that no clear ellipsoid structures (**see ESI Figure S2 for TEM images**) formed

14   when the conventional heating flow reactor was used, the self-assembly of primary hematite

15   nanocrystals to form stable ellipsoid Hem-SSs is regarded to be induced by microwave

16   irradiation (**Figure 6a-b**). The surprising effect of microwave heating on the oriented

17   attachment of pre-synthesized α-Fe$_2$O$_3$ nanoparticles to form large and crystalline ellipsoidal

18   α-Fe$_2$O$_3$ nanocrystals was also reported when in a batch reactor.[33] α-Fe$_2$O$_3$ nanoparticles are

19   known to have magnetic moment that creates dipole–dipole attractions and they can act as

20   antennas and absorb the microwave irradiation selectively.[34, 35] In an electromagnetic field

21   generated by microwave irradiation, α-Fe$_2$O$_3$ nanoparticles are highly polarized and localized

22   currents are probably created on the "hot surfaces" of α-Fe$_2$O$_3$ nanoparticles.[35]

23   In order to further understand the effect of microwave irradiation to ellipsoid Hem-SSs

24   formation, control experiments were performed using a microwave batch reactor. In a typical

25   control experiment, 3 mL of aqueous precursor solution (0.05, 0.1 and 0.2 mol L^{-1}

1　Fe(NO$_3$)$_3$.9H$_2$O) was irradiated by microwave for 6 min at 120 ^{o}C without stirring. At low

2　concentration (0.05 mol L^{-1} Fe(NO$_3$)$_3$.9H$_2$O), particles could not be isolated. Hematites,

3　characterised by UV-vis spectroscopy, were produced successfully when high concentration

4　of precursor (0.1 and 0.2 mol L^{-1}) was used (**ESI Figure S5a**). Produced particles were

5　isolated and further analysed by TEM. In contrast to ellipsoid Hem-SSs synthesized by

6　MWPF system, few ellipsoid particles with irregular morphologies were produced by

7　microwave batch reactor without stirring. (**ESI Figure S5b-f**), which is partially　in

8　agreement with the literature that reported ellipsoid α-Fe$_2$O$_3$ formation could take place under

9　microwave heating in batch reactor.[33] It is also worth noting that ellipsoids were obviously

10　formed at high precursor concentration in this study, indicating microwave irradiation can

11　produce ellipsoid but the yield is relative moderate due to limited penetration depth of

12　microwave in a batch reactor.

13　A microwave induced nucleation-aggregation mechanism followed by an oriented attachment

14　of primary α-Fe$_2$O$_3$ nanoparticles and Oswald ripening may be proposed for the formation of

15　Hem-SSs, although the exact mechanism of the formation at present remains unclear. As

16　shown in **Figure 6b**, firstly goethite nanocrystals, α-FeO(OH) are probably generated by the

17　microwave induced forced hydrolysis of Fe(NO$_3$)$_3$.9H$_2$O.[36, 37] Due to their high surface

18　energy these freshly formed nanocrystals probably aggregate rapidly in a random manner and

19　subsequently undergo dehydration to form primary α-Fe$_2$O$_3$ nanoparticles.[37] Meanwhile,

20　microscopic "hot surfaces" created on particles probably accelerate the crystal growth.

21　Produced primary nanoparticles are subsequently highly polarized under microwave

22　irradiation (2.45 GHz) due to their excellent microwave absorbing characteristic and become

23　energetically more excited.[34] Highly polarized activated primary α-Fe$_2$O$_3$ nanoparticles form

24　due to generated dipole-dipole attractions[29] and start oriented attachment to produce Hem-

25　SSs.[38-41]　In addition, the smooth surface of ellipsoid Hem-SSs observed by TEM is thought

1 to be due to Oswald ripening after the oriented attachment of primary α-Fe_2O_3

2 nanoparticles.[36, 41] The oriented attachment process however leads to formation of ellipsoid

3 Hem-SSs morphologies, which may be related to both the distortion of internal charges in

4 nanoparticle crystal structure to polarize against the external field generated by microwave

5 irradiation and the increased mass of assembled Hem-SSs that affects the particle motion

6 under constant buoyant force of water. The reason behind the stability of hierarchical Hem-

7 SSs formed and the absence of crystallographic fusion to single-crystals is still unknown.

8 However, it could be attributed to both the shape of primary hematite nanoparticles and the

9 residence time of Hem-SSs in the reactor and needs further investigation.

10

1
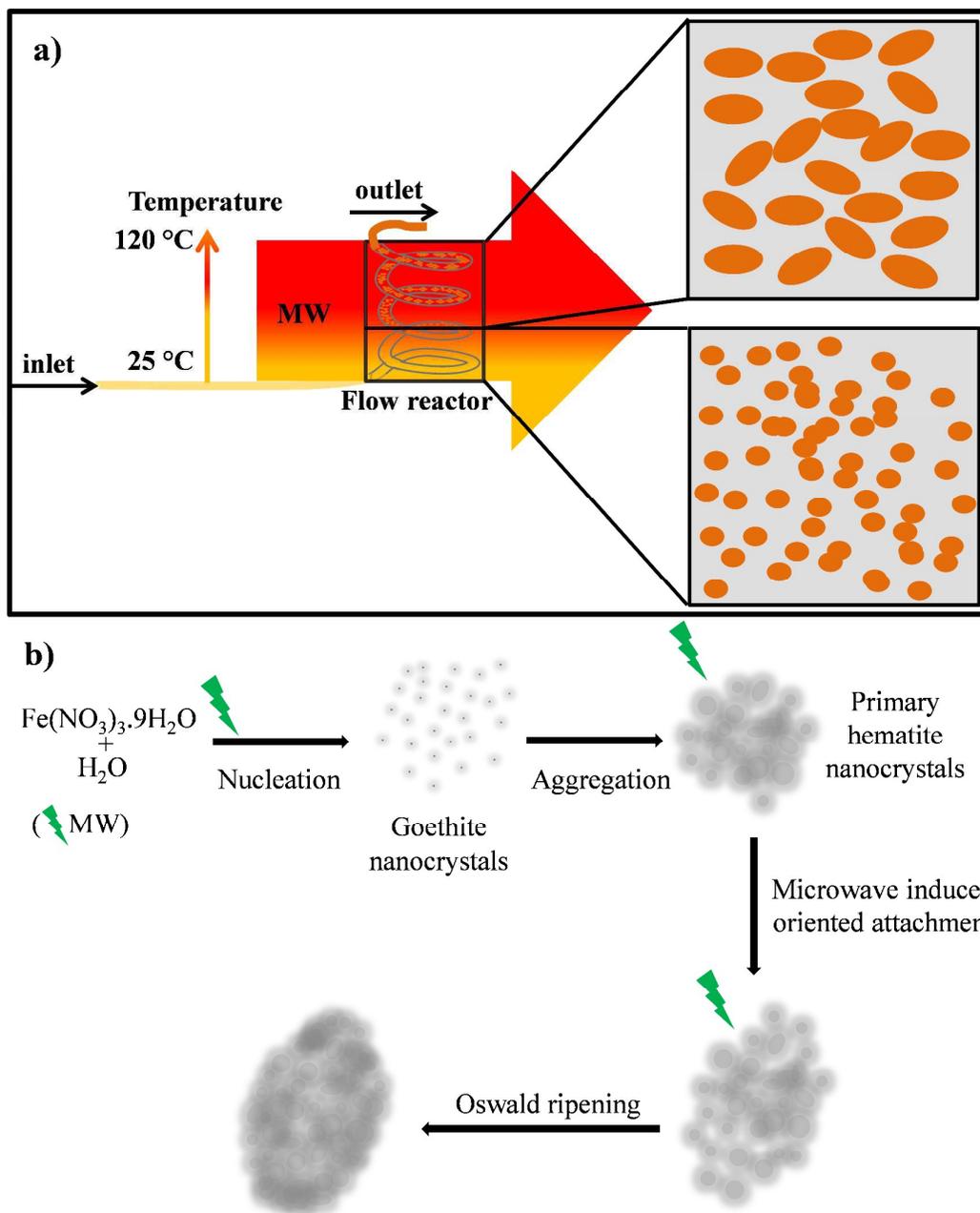
Figure 6 Schematic representation of proposed mechanism for microwave assisted directed

self-assembly of primary hematite nanoparticles to form Hem-SSs. (**a**) Fabrication of primary

hematite nanocrystals while travelling in the flow reactor (bottom square). Directed self-

assembly of primary hematite nanoparticles under continuous microwave irradiation (top

square). Colour change on the arrow (yellow to red) shows the possible temperature change

throughout the flow reactor. (**b**) Proposed mechanism scheme for the formation of Hem-SSs.

1 **Conclusions**

2 Pure and crystalline ellipsoid hematite superstructures were fabricated in ~6 min time without

3 employing surfactants or templates in a MWPF system using $Fe(NO_3)_3.9H_2O$ as the only

4 precursor. Microwave irradiation is thought to direct the self-assembly of produced hematite

5 subunits via selective heating and polarization of nanoparticles. Concentration and flow rate

6 of the precursor solution were found to be critical for Hem-SS synthesis. Less crystalline

7 hematite formation was observed at high precursor concentrations (0.1 and 0.2 mol L^{-1}). No

8 hematite particle formation was observed at higher flow rates, indicating the significance of

9 the amount of microwave energy absorbed per unit time. Conversely, CH was not able to

10 produce pure hematite under identical conditions at 120 and even at 140 °C. The developed

11 sustainable process that benefits from both MH and flow technology is reproducible and has

12 the potential to fabricate other metal/metal oxide nanoparticles or their self-assembled

13 superstructures, core/shell structures and hybrid nanomaterials.

14 **Acknowledgements**

16

17 **References**

18 1.   R.-Q. Song and H. Cölfen, *Advanced Materials*, 2010, **22**, 1301-1330.
19 2.   H. Cölfen and M. Antonietti, *Angew. Chem. Int. Ed.*, 2005, **44**, 5576-5591.
20 3.   L. Bergström, E. V. Sturm, G. Salazar-Alvarez and H. Cölfen, *Accounts of Chemical*
21   *Research*, 2015, **48**, 1391-1402.
22 4.   M.-G. Ma and H. Cölfen, *Current Opinion in Colloid & Interface Science*, 2014, **19**,
23   56-65.
24 5.   T. Tachikawa and T. Majima, *NPG Asia Mater*, 2014, **6**, e100.
25 6.   X. Duan, L. Mei, J. Ma, Q. Li, T. Wang and W. Zheng, *Chemical Communications*,
26   2012, **48**, 12204-12206.
27 7.   Z. An, J. Zhang, S. Pan and F. Yu, *The Journal of Physical Chemistry C*, 2009, **113**,
28   8092-8096.
29 8.   X. Fei, W. Li, Z. Shao, S. Seeger, D. Zhao and X. Chen, *Journal of the American*
30   *Chemical Society*, 2014, **136**, 15781-15786.
31 9.   J. Ma, J. Teo, L. Mei, Z. Zhong, Q. Li, T. Wang, X. Duan, J. Lian and W. Zheng, *Journal*
32   *of Materials Chemistry*, 2012, **22**, 11694-11700.
33 10.   X.-L. Fang, C. Chen, M.-S. Jin, Q. Kuang, Z.-X. Xie, S.-Y. Xie, R.-B. Huang and L.-S.
34   Zheng, *Journal of Materials Chemistry*, 2009, **19**, 6154-6160.

11. F. Jiao, J.-C. Jumas, M. Womes, A. V. Chadwick, A. Harrison and P. G. Bruce, *Journal of the American Chemical Society*, 2006, **128**, 12905-12909.

12. M. Zhu, Y. Wang, D. Meng, X. Qin and G. Diao, *Journal of Physical Chemistry C*, 2012, **116**, 16276-16285.

13. H.-J. Kim, K.-I. Choi, A. Pan, I.-D. Kim, H.-R. Kim, K.-M. Kim, C. W. Na, G. Cao and J.-H. Lee, *Journal of Materials Chemistry*, 2011, **21**, 6549-6555.

14. W. T. Dong and C. S. Zhu, *Journal of Materials Chemistry*, 2002, **12**, 1676-1683.

15. P. M. Kouotou, Z.-Y. Tian, H. Vieker and K. Kohse-Hoeinghaus, *Surface & Coatings Technology*, 2013, **230**, 59-65.

16. G. Qiu, H. Huang, H. Genuino, N. Opembe, L. Stafford, S. Dharmarathna and S. L. Suib, *The Journal of Physical Chemistry C*, 2011, **115**, 19626-19631.

17. A. Abou-Hassan, O. Sandre and V. Cabuil, *Angew. Chem. Int. Ed.*, 2010, **49**, 6268-6286.

18. M. Nishioka, M. Miyakawa, Y. Daino, H. Kataoka, H. Koda, K. Sato and T. M. Suzuki, *Industrial & Engineering Chemistry Research*, 2013, **52**, 4683-4687.

19. M. Nishioka, M. Miyakawa, H. Kataoka, H. Koda, K. Sato and T. M. Suzuki, *Nanoscale*, 2011, **3**, 2621-2626.

20. S. Horikoshi, H. Abe, K. Torigoe, M. Abe and N. Serpone, *Nanoscale*, 2010, **2**, 1441-1447.

21. S. Horikoshi, T. Sumi and N. Serpone, *Chemical Engineering and Processing: Process Intensification*, 2013, **73**, 59-66.

22. T. Fujii, F. M. F. de Groot, G. A. Sawatzky, F. C. Voogt, T. Hibma and K. Okada, *Physical Review B*, 1999, **59**, 3195-3202.

23. A. A. Tahir, K. G. U. Wijayantha, S. Saremi-Yarahmadi, M. Mazhar and V. McKee, *Chemistry of Materials*, 2009, **21**, 3763-3772.

24. D. A. Wheeler, G. Wang, Y. Ling, Y. Li and J. Z. Zhang, *Energy & Environmental Science*, 2012, **5**, 6682-6702.

25. K. Sivula, R. Zboril, F. Le Formal, R. Robert, A. Weidenkaff, J. Tucek, J. Frydrych and M. Grätzel, *Journal of the American Chemical Society*, 2010, **132**, 7436-7444.

26. D. L. A. de Faria, S. Venâncio Silva and M. T. de Oliveira, *Journal of Raman Spectroscopy*, 1997, **28**, 873-878.

27. M. Hanesch, *Geophysical Journal International*, 2009, **177**, 941-948.

28. J.-M. Meijer, D. V. Byelov, L. Rossi, A. Snigirev, I. Snigireva, A. P. Philipse and A. V. Petukhov, *Soft Matter*, 2013, **9**, 10729-10738.

29. M. Grzelczak, J. Vermant, E. M. Furst and L. M. Liz-Marzán, *ACS Nano*, 2010, **4**, 3591-3605.

30. C.-W. Wang, D. Sinton and M. G. Moffitt, *Journal of the American Chemical Society*, 2011, **133**, 18853-18864.

31. X. Zhang, K. D. Harris, N. L. Y. Wu, J. N. Murphy and J. M. Buriak, *ACS Nano*, 2010, **4**, 7021-7029.

32. J. Vermant and M. J. Solomon, *Journal of Physics: Condensed Matter*, 2005, **17**, R187.

33. W.-W. Wang, Y.-J. Zhu and M.-L. Ruan, *Journal of Nanoparticle Research*, 2007, **9**, 419-426.

34. T. Druzhinina, W. Weltjens, S. Hoeppener and U. S. Schubert, *Advanced Functional Materials*, 2009, **19**, 1287-1292.

35. X. Hu, J. C. Yu, J. Gong, Q. Li and G. Li, *Advanced Materials*, 2007, **19**, 2324-2329.

36. U. Schwertmann, J. Friedl and H. Stanjek, *Journal of Colloid and Interface Science*, 1999, **209**, 215-223.

1   37.   J. F. Banfield, S. A. Welch, H. Zhang, T. T. Ebert and R. L. Penn, *Science*, 2000, **289**,
2   751-754.
3   38.   M. Ocaña, M. P. Morales and C. J. Serna, *Journal of Colloid and Interface Science*,
4   1995, **171**, 85-91.
5   39.   A. P. Alivisatos, *Science*, 2000, **289**, 736-737.
6   40.   M. Adachi, Y. Murata, J. Takao, J. Jiu, M. Sakamoto and F. Wang, *Journal of the*
7   *American Chemical Society*, 2004, **126**, 14943-14949.
8   41.   Y. Cheng, Y. Wang, D. Chen and F. Bao, *The Journal of Physical Chemistry B*, 2005,
9   **109**, 794-798.

10